Clinical Imaging 72 (2021) 162–167

Contents lists available at ScienceDirect

Clinical Imaging

journal homepage: www.elsevier.com/locate/clinimag

Neuroradiology

Multiple Sclerosis lesions detection by a hybrid Watershed-Clustering algorithm

Lilla Bonanno, Nadia Mammone, Simona De Salvo *, Alessia Bramanti, Carmela Rifici, Edoardo Sessa, Placido Bramanti, Silvia Marino, Rosella Ciurleo

IRCCS Centro Neurolesi "Bonino-Pulejo", Messina, Italy

ARTICLE INFO

Keywords:
Watershed algorithm
Image segmentation
Magnetic Resonance Imaging
Multiple Sclerosis
CAD system

ABSTRACT

Background: Computer Aided Diagnosis (CAD) systems have been developing in the last years with the aim of helping the diagnosis and monitoring of several diseases. We present a novel CAD system based on a hybrid Watershed-Clustering algorithm for the detection of lesions in Multiple Sclerosis.
Methods: Magnetic Resonance Imaging scans (FLAIR sequences without gadolinium) of 20 patients affected by Multiple Sclerosis with hyperintense lesions were studied. The CAD system consisted of the following automated processing steps: images recording, automated segmentation based on the Watershed algorithm, detection of lesions, extraction of both dynamic and morphological features, and classification of lesions by Cluster Analysis.
Results: The investigation was performed on 316 suspect regions including 255 lesion and 61 non-lesion cases. The Receiver Operating Characteristic analysis revealed a highly significant difference between lesions and non-lesions; the diagnostic accuracy was 87% (95% CI: 0.83–0.90), with an appropriate cut-off of 192.8; the sensitivity was 77% and the specificity was 87%.
Conclusions: In conclusion, we developed a CAD system by using a modified algorithm for automated image segmentation which may discriminate MS lesions from non-lesions. The proposed method generates a detection out-put that may be support the clinical evaluation.

1. Introduction

Multiple Sclerosis (MS) is a chronic autoimmune disease characterized by multiple demyelination lesions in the spinal cord and in the white matter of the brain [1]. Magnetic Resonance Imaging (MRI) plays an important role as a non-invasive diagnostic tool to establish the diagnosis of demyelinating MS lesions [2]. Indeed, the characteristic MS abnormalities detected by MRI consist in multiple white matter lesions with high signal intensity on Fluid Attenuation Inversion Recovery (FLAIR), Proton Density weighted (PD), and T2-weighted sequences and low signal intensity on T1-weighted sequence [3]. However, in some cases, as reported in literature, the poor optimization, due to magnetic field intensity of Magnetic Resonance tool could not allow to detect MS lesions with facility and rapidity (referring to signal inhomogeneity induced by B1 inhomogeneity and coil sensitivity variations across the field of view), especially in conditions of pre-existing lesion burden [4]. For this reason, Computer Aided Diagnosis (CAD) methods have been developed to support the radiologist in detection of potential MRI abnormalities in reliable manner and efficient time [5]. We have developed a CAD software tool by using a hybrid algorithm based on the joint use of Watershed and Cluster Analysis in order to discriminate the MS lesions from non-lesions and to pinpoint their location. The watershed segmentation generates spatially homogeneous regions which are oversegmented. But we applied cluster analysis to solve the problem of undesirable oversegmentation results produced by the watershed technique. In our previous study [6], we proposed a CAD system able to discriminate carotid atherosclerotic plaques from non-plaques and to identify their location in the Ultrasound (US) images. In the present research, a CAD system has been developed for MR images with the purpose to support the clinician in MS lesion detection. The method previously introduced [6,7] has been hereby optimized for MR image analysis. Our approach to the development of a CAD system for MR images differs from the CAD system in US because it requires pre-processing for artifact reduction and utilizes Complete Linkage rather than Ward's method for cluster analysis. The first difference between the two methods is that US images can be easily enhanced by a single

* Corresponding author at: IRCCS Centro Neurolesi "Bonino-Pulejo", S.S. 113, Via Palermo, Cda. Casazza, 98124 Messina, Italy.
E-mail address: simona.desalvo@irccsme.it (S. De Salvo).

https://doi.org/10.1016/j.clinimag.2020.11.006
Received 24 March 2020; Received in revised form 21 September 2020; Accepted 2 November 2020
Available online 5 November 2020

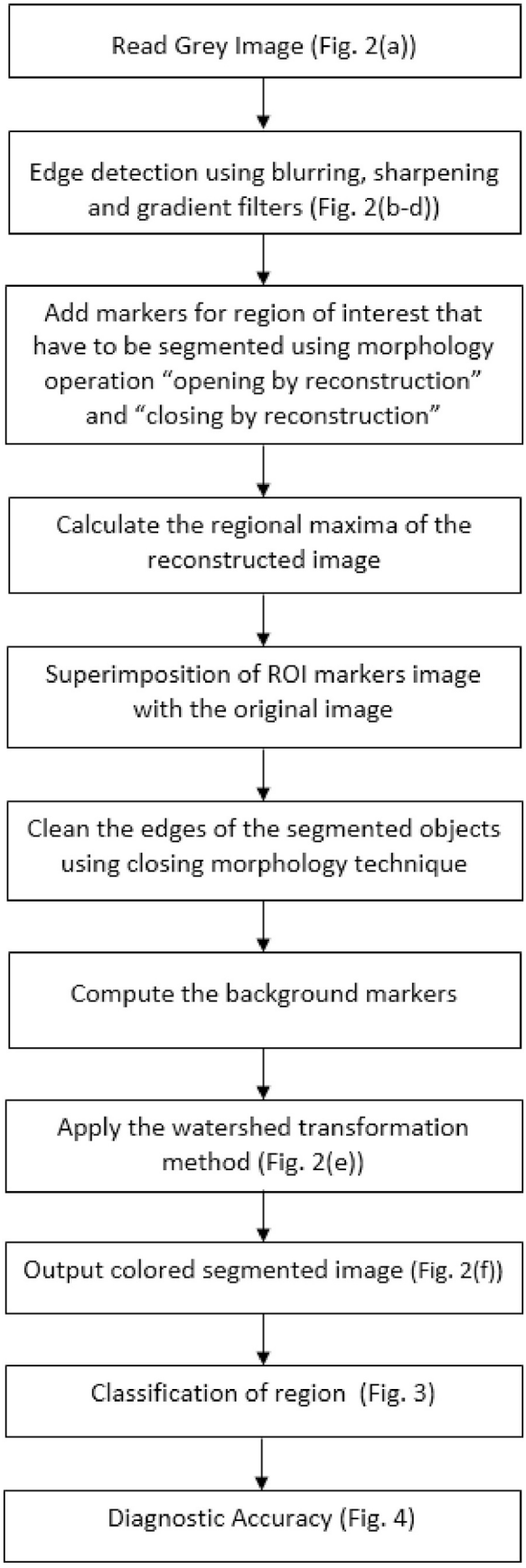

Fig. 1. Flow diagram of CAD system. Step of hybrid algorithm.

filtering step, whereas MR images require a multistep pre-processing in order to properly reduce the artifacts. Indeed, a particular combination of blurring, sharpening and gradient filters was applied. Another difference is that the proposed hybrid algorithm is based on a different cluster analysis methodology. Indeed, in ultrasound images we applied the Ward's method [6,7]. In the present study, we adopted the Complete Linkage because it allows overcoming the problem of over segmentation of MRI. The objective of this work is to apply cluster analysis to provide a repeatable and objective tool to support the clinicians in the quantification and identification of MS lesions.

2. Materials and methods

This is a retrospective study in which was analyzed MR images of 20 patients with relapsing remitting MS. We considered the MRI examinations of the cases that fulfilled the following criteria: i) Barkhof criteria (new MS diagnostic criteria adopted to demonstrate the dissemination of lesions in space on conventional MRI [8]); ii) not relapses and not corticosteroid treatments in the three months preceding the scanning. No ethical committee approval was necessary according to national regulations because this was a retrospective analysis of routinely collected anonymized clinical data. The radiologist interpretation highlighted on the MRI, in particular in T2 FLAIR sequence, the hyperintense lesions in the periventricular white matter region (in particular in the superior and posterior regions of the corona radiata). Given the set of parameters extracted from each ROI, we taken into account particularly the average signal intensity of each region, because it could be an indicator able to discriminate lesions from non-lesions.

2.1. Magnetic Resonance Imaging

MRI examinations were performed with a scanner operating at 1.5 T (Siemens Sonata). The following sequences were requirements for inclusion in this study: i) sagittal T1-weighted images, acquired to define the anterior-posterior commissural plane; ii) T2 FLAIR images (TR = 9000 msec; TE = 150 msec; 50 contiguous 3 mm slices) which improves the detection of lesions within the subarachnoid space and brain parenchyma, particularly the lesions near the brain-cerebral spinal fluid interface [9]. Twenty T2 FLAIR images of MS patients were fed into the algorithm which processed them automatically and sequentially.

2.2. Lesion segmentation algorithm

The series were then anonymized and transferred to the CAD system as Digital Imaging and Communications in Medicine (DICOM) files. The CAD system implemented the following sequence of processing steps: segmentation and detection of lesions, extraction of morphological features, and finally lesion classification (Fig. 1). The proposed method was applied to the dataset of 20 MR images of each patients and compared with the opinion of an expert neurologist (golden standard). The analysis of images was carried out automatically, without no need of any user-interaction. The hybrid Watershed-Clustering algorithm was implemented using MATLAB 7.6. The accuracy analysis was performed using the software R. Through the Shapiro-Wilk test (1965) the assumption of normality of the estimated variables of both lesion and non-lesion groups was assessed. We have calculated the DICE coefficient to observe the deviation between manual segmentation (expert neurologist) and automatic segmentation (algorithm) and we obtained 0.95 ± 0.03 which indicates almost complete overlap.

2.3. Pre-processing

Brain MR image segmentation is challenging because of variable imaging parameters, noise, overlapping intensities, motion, gradients, blurring, susceptibility artifacts and normal anatomical variability [10]. Thus, two pre-processing steps should normally precede any approach to

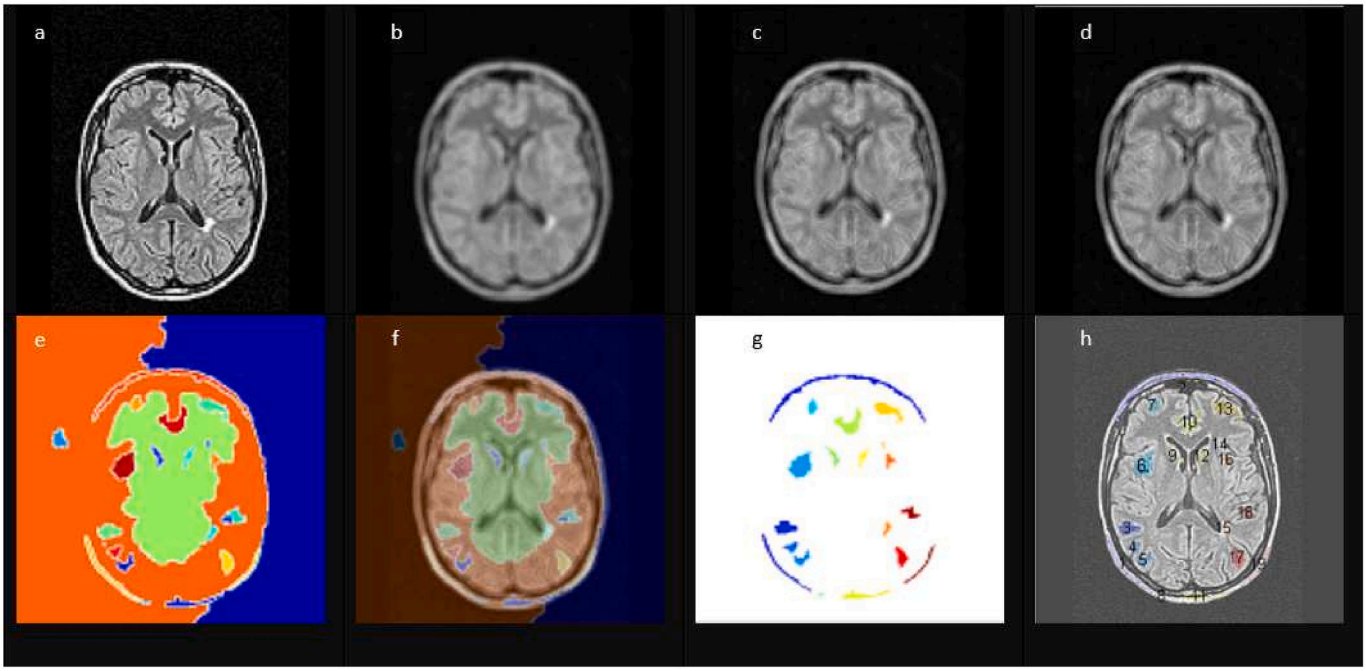

Fig. 2. Output of algorithm. (a) Original Image; (b) edge detection using blurring filter; (c) edge detection using sharpening filter; (d) edge detection using gradient filter; (e) application of the watershed transformation method; (f) output of the colored segmented image; (g) regions that satisfy the condition imposed on the ratio of average signal intensity; (h) application of results on original image.

MS lesion segmentation: first, removal of image artifact; second, subtraction of non-brain tissues from the image, such as scalp and skull. The Fig. 2 shows an example of Watershed algorithm application to one of 20 patients. As the aim was to maximize the performance of image segmentation, removing image inhomogeneities generated by field bias and suppressing the random noise generated by digital acquisition was necessary. Specific filters for the removal of artifacts from the early image were applied (Fig. 2(a)). First of all, a blurring filtering was applied in order to reduce noise; the resulting blurred image needed a contrast enhancement that was carried out by the sharpening filter; in the end, a gradient filter provided information about the direction of the most rapid change in gray scale intensity.

In particular, a blurring filter allowed attenuating the changes of luminosity in the neighborhood of a pixel. A blurring measure allowed an objective blur estimation by computing the width average of all horizontal and vertical edges in the image. The found width was accumulated in a total edge width counter and then divided between the number of borders found. In our algorithm we used a blurring filter with 4px radius; it defines the value of the standard deviation to the Gaussian function, i.e., how many pixels on the screen blend into each other; thus, a larger value creates more blur (Fig. 2(b)); a sharpening filter increased the local contrast of the sharpness (Fig. 2(c)); radius was the standard deviation of the Gaussian lowpass filter set at 1 for sharpening narrower regions around edges. This value controls the size of the region around the edge pixels to increase sharpening. Typical values for this parameter are within the range [0 2]; very large values for this parameter may create undesirable effects in the output image.

Finally, we applied a Sobel filter to detect edges in the image. The Sobel operator calculates the gradient of image intensity at each point, giving the directional gradient along x-axis (horizontal), specified as a numeric matrix equal in size to image I, and directional gradient along y-axis (vertical), specified as a numeric matrix equal in size to image I. This procedure allowed for extracting the contours and the image (Fig. 2 (d)).

Images can be automatically segmented into visually sensible regions by finding the watershed regions in a gradient magnitude image.

2.4. Processing

As previously described [7], the floodings algorithm [11] was exploited in order to determine lesions foreground in the image by means of Watershed algorithm. If the early grayscale image is denoted as I of the discrete plane $\mathbb{Z}^2$ into a discrete set {1, …, N}, where N is the number of pixels, the gradient image ΔI is then estimated. The concept of Watershed is based on visualizing an image in three dimensions: two spatial coordinates versus gray levels. For a particular regional minimum, the set of points at which a drop of water, if placed at the location of any of those points, would fall with certainty to a single minimum, is called the *catchment basin* or *Watershed* of that minimum. Crest lines on the topographic surface and are termed *divide lines* or *Watershed lines*. Direct application of watershed algorithm to the gradient images produce unreliable image segmentation, because of the presence of several local minima due to the noise present in real (gradient) images. One way to reduce the presence of false regions is the so-called "marker image" technique, which consists in delineating automatically those regions that require segmentation, even though it is generally challenging to obtain relevant markers with no interaction with the user [12]. In this paper, the markers were determined by using the morphology operation technique, which is totally automatic, called "opening by reconstruction and closing by reconstruction" to remove the small blemishes without affecting the overall shape of the segmented lesions. Erosion-based gray-scale reconstruction was used (Eq. (1)):

$$\phi_I^{(rec)}(J) = \bigcap_{n\geq 1} \varepsilon^{(n)}(J) \tag{1}$$

$\varepsilon^{(n)}(J)$ is calculated by iterating n elementary geodesic erosion, where the geodesic erosion is defined as (Eq. (2)):

$$\varepsilon^{(I)}(J) = (J \ominus b) \cup I \tag{2}$$

b is a flat structuring element with the same size as the matrix I (256*256), $\ominus$ erosion and $\cup$ represents the pointwise maximum.

The next step is dilation-based gray-scale reconstruction (Eq. (3)):

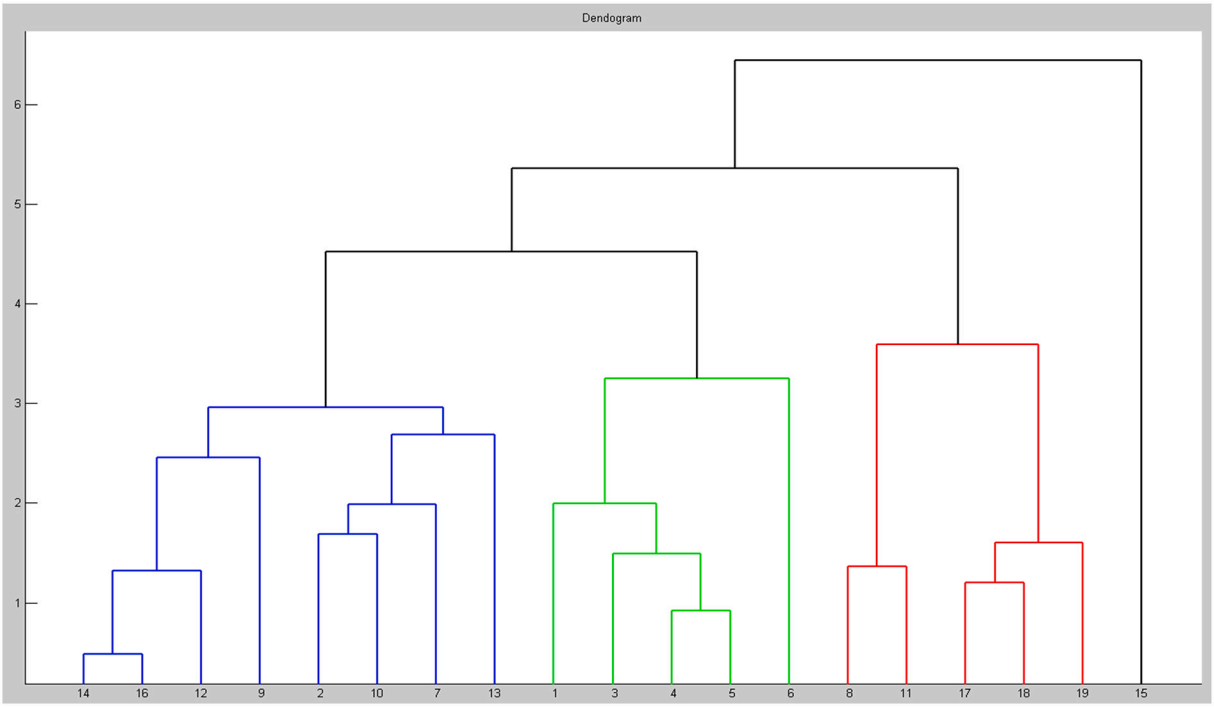

Fig. 3. Dendrogram representation. The dendrogram shows that the region 15 is isolated from other regions. This means that the region has not similar characteristics to be grouped with other regions.

$$\gamma_I^{(rec)}(J) = \bigcup_{n\geq 1} \delta^{(n)}(J) \tag{3}$$

where $\delta^{(n)}(J)$ is calculated by iterating n elementary geodesic dilations, where the geodesic dilation is defined as (Eq. (4)):

$$\delta^{(I)}(J) = (J \oplus b) \cap I \tag{4}$$

b is the flat structuring element of size I, $\oplus$ direct sum and $\cap$ represents the pointwise minimum.

The aforementioned techniques are more effective in removing small blemishes while preserving the shape of the lesions. In order to get foreground lesions with smooth edges, the regional maxima of these reconstructed images were estimated. Then, background markers were determined and watershed transform of segmentation function was applied (Fig. 2(e)). Finally, the pseudo-color label matrix was overlapped to the original intensity image (Fig. 2(f)). Successively, cluster analysis was applied to solve the problem of undesirable oversegmentation results produced by the watershed technique.

2.5. Feature extraction

To describe the morphological features of the image, 13 shape based and texture parameters were calculated, as described previously [7]. The parameters which are normally taken into account by clinicians to describe the morphology of lesions were extracted from each Region Of Interest (ROI): Area; Perimeter; Distance; Average Signal Intensity; Centroid; Eccentricity; Euler Number; Filled Area; Extent; Solidity; Orientation; Equivalent Diameter.

Let define the Average Signal Intensity Feature (ASIF) as (Eq. (5)):

$$ASIF = \frac{Mean\ Intensity_{single\ region}}{Mean\ Intensity_{image}} \tag{5}$$

When $ASIF \geq 1$, the region is labeled as "suspicious region" and only a minimal set of three parameters were used as input to the classifier: average distance of image center, average signal intensity and coordinates of contour pixel (Fig. 2(g–h)). Successively, cluster analysis was applied to solve the problem of undesirable oversegmentation results produced by the watershed technique.

2.6. Classification

The algorithm then evaluates the ASIF for each ROI. It normalizes and classifies a ROI according to ASIF into a number of different groups so that similar lesions are clustered together in the same group. The city blocks norms were applied to perform the clustering (Eq. (6)):

$$d(i,h) = \sum_j |x_{ij} - x_{hj}| \tag{6}$$

The Complete Linkage was selected as distance measure to aggregate clusters (Eq. (7)):

$$d(A,B) = max(d(i,h)) \tag{7}$$

The output diagram, the so-called "dendrogram", represents how clusters were joined at each stage of the analysis as a function of the distance between clusters at the time of joining (Fig. 3).

2.7. Diagnostic accuracy

In order to calculate the diagnostic accuracy (Area Under the ROC curve, AUC) of the CAD (under the null hypothesis: AUC = 0.5), with an appropriate cut-off, Receiver Operating Characteristic (ROC) analysis was performed. The results achieved on the dataset of 20 MR images containing MS lesions were compared with the opinion of an expert neuroradiologist (golden standard). The expert neuroradiologist blindly reviewed the images and manually marked the centers of the lesions that he could visually detect. The output of the algorithm was evaluated in the following way:

- The center of a given lesion falls within a region labeled by the algorithm as "lesion" (true positive);
- No center of lesion falls within a given region labeled by the algorithm as "lesion" (false positive);

Table 1
ROC analysis data.

Threshold	Sensitivity (95% CI)	Specificity (95% CI)	PPV (95% CI)	NPV (95% CI)
192.8	77 (64.5–86.8)	87 (82.3–90.9)	58.7 (47.1–69.7)	94.1 (90.2–96.7)

Legend: CI = Confidence Interval.

- The center of a given lesion falls within no region labeled by the algorithm as "lesion" (false negative);
- No center of lesion falls within a region labeled by the algorithm as "non lesion" (true negative);

Sensitivity and specificity were assessed with a 95% confidence interval (CI). A *p*-value smaller than 0.05 (two-sided) were considered statistically significant.

3. Results

We analyzed the T2 FLIR of 20 patients with relapsing remitting MS (9 females and 11 males; mean age: 32 years [range 19–47 years]; median EDSS: 2 [range 0–5.5]).

The method segmented 316 regions; 255 out of 316 were classified as non-lesions and had an average signal intensity of 174.3 (SD = 17.9), whereas 61 out of 316 were classified as lesions and had an average signal intensity of 242.4 (SD = 26.97). Both groups (W = 0.98, $p = 0.005$ non-lesion group; W = 0.96, $p = 0.03$ lesion group) resulted not normally distributed. A hypothesis test of interest was whether the level of average signal intensity was able to distinguish between the two groups. This problem was formulated statistically in terms of AUC (Area Under the Curve). The level of ASIF was measured on a continuous scale with observations on the two independent groups. The area under the curve was equal to 0.87; this means that the marker should be considered moderately accurate, according to the classification of Swets [13]. The next aim was to determine the threshold value that allowed for discrimination between the two groups. The threshold is determined by the optimal cut-point of the ROC curve, according to the method described in [14]. In this case, the statistical tests showed that in according to the Youden index, the optimal cut-off value was k = 192.8 (Table 1).

The ROC analysis unveiled a highly significant AUC difference in the discrimination between lesions and non-lesions: the diagnostic accuracy was 87% (95% CI: 0.83 0.90), an appropriate cut-off value was 192.8, the sensitivity was 77% and the specificity reached 87% (Fig. 4). The present results show that the proposed computerized method may help to discriminate the lesions from non-lesions in T2 FLAIR MR sequences.

4. Discussion

The present study introduced a CAD system able to discriminate MS lesions from non-lesions and to identify their location in the MRI scans by using T2 FLAIR sequences. The set of MRI images was first preprocessed to remove artifacts. The proposed method exploited adaptive filters to enhance structures within the MS lesion and then it identified the structures by applying a Watershed algorithm. ROIs based on the detected MS lesions were extracted from each MR image, and a set of meaningful features were estimated for each extracted ROI. Cluster Analysis was applied to deal with the issue of undesirable oversegmentation produced by the watershed algorithm. Cluster analysis also allowed reducing the number of false detections. The results of ROC curve analysis suggest that the proposed algorithm may be particularly helpful for identifying lesions. The preliminary experimental results on 316 segmented regions prove that the proposed method is able to detect and classify correctly the lesions with a diagnostic accuracy of 87%. Signal intensity of lesions and non-lesions resulted significantly different. Moreover, we calculated the DICE coefficient to highlight the difference between manual and automated segmentation in according to Carass et al. study [15].

Automated methods of detection, identification and quantification of MS lesions were presented by many researchers [16–18]. Golberg et al. [16] used the automatic method and they obtained a specificity of 87% and a specificity of 96%. However, they used T2-weighted with gadolinium images. Some investigators showed that semiautomatic CAD methods outperformed manual ROI techniques [19,20]. In general, marketable CAD systems rely on an enhanced threshold, where lesions exhibiting an initial enhancement below this threshold are not coded [21,22]. The results of our method favorably compare to those one obtained by Baltzer et al. [21], who reported that the performance of a semiautomatic CAD system achieved an AUC of 83%, with an enhanced

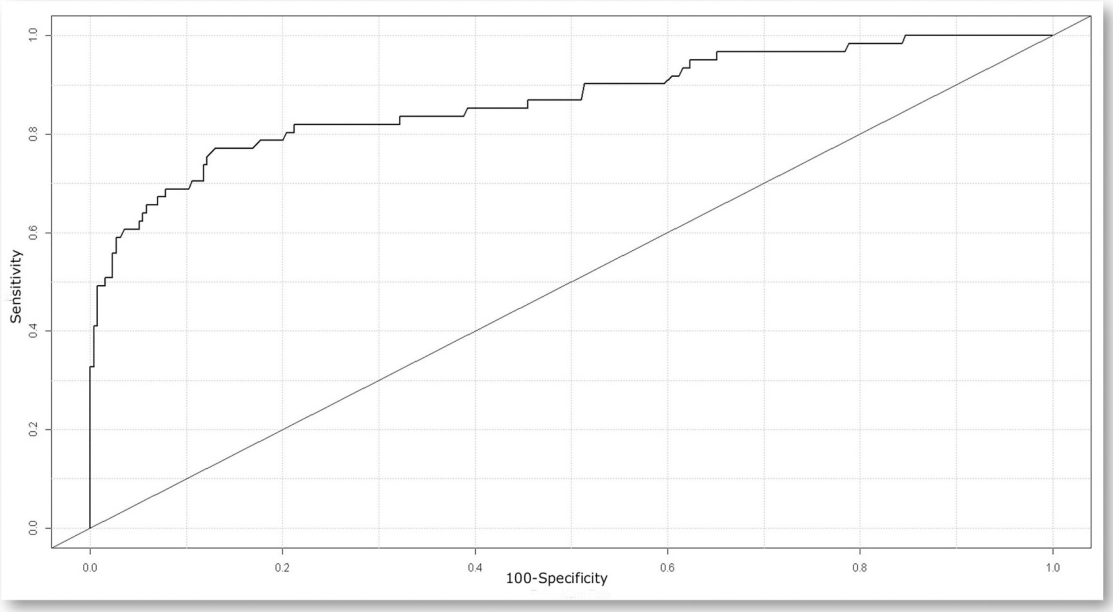

Fig. 4. The ROC curve for average signal intensity. The value of classification results produced the best performance with an AUC value of 0.87.

threshold of 33%. Nevertheless, the method proposed by Baltzer et al. [21] was user-dependent and was applied on gadolinium images. The method proposed in the present study achieved an AUC of 87%, giving better results and in a fully automatic manner. Moreover, it is the only one currently using an automatic hybrid algorithm to segment MS lesions with a good accuracy, based on T2 FLAIR images without gadolinium. The innovation lies in uniting the watershed algorithm and cluster analysis to overcome the problem of over segmentation.

5. Conclusions

In conclusion, the developed CAD system for RM image analysis can discriminate MS lesions from non-lesions with high accuracy (87%) by using an algorithm for automated segmentation. The computer extracted average signal intensity features and the final classification discriminated between lesions and non-lesions significantly. Observer independent CAD may therefore be a promising tool for interpreting MS lesions in MR images. The next step of our research will apply this method on images coming from MR with a high field which provides a better resolution of the image.

Funding

This research did not receive any specific grant from funding agencies in the public, commercial, or not-for-profit sectors.

Declaration of competing interest

None.

Acknowledgments

None.

References

[1] Lucchinetti CF, Popescu BFG, Bunyan RF, et al. Inflammatory cortical demyelination in early multiple sclerosis. N Engl J Med 2011;325:2188–97.
[2] Traboulsee A, Li DK, Zhao G, Paty DW. Conventional MRI techniques in multiple sclerosis. In: MR imaging in white matter diseases of the brain and spinal cord. Springer; 2005. 211:221–223.
[3] Gawne-Cain ML, Silver NC, Moseley IF, Miller DH. Fast FLAIR of the brain: the range of appearances in normal subjects and its application to quantification of white-matter disease. Neuroradiology 1997;39:243–9.
[4] Bilello M, Arkuszewski M, Nucifora P, Nasrallah I, Melhem ER, Cirillo L, et al. Multiple sclerosis: identification of temporal changes in brain lesions with computer-assisted detection software. Neuroradiol J 2013;26:43–150.
[5] Castellino RA. Computer aided detection (CAD): an overview. Cancer Imaging 2005;5:17–9.
[6] Bonanno L, Marino S, Bramanti P, Sottile F. Validation of a computer-aided diagnosis system for the automatic identification of carotid atherosclerosis. Ultrasound in Medicine and Biology 2015;41:509–16.
[7] Sottile F, Marino S, Bramanti P, Bonanno L. Validating a computer-aided diagnosis system for identifying carotid atherosclerosis. In: Image and signal processing (CISP). 6th international congress. 2; 2013. p. 641–5.
[8] Sastre-Garriga J, Tintoré M, Rovira A, Nos C, Río J, Thompson AJ, et al. Specificity of Barkhof criteria in predicting conversion to multiple sclerosis when applied to clinically isolated brainstem syndromes. Arch Neurol 2004;61:222–4.
[9] Stuckey SL, Goh TD, Heffernan T, Rowan D. Hyperintensity in the subarachnoid space on FLAIR MRI. Am J Roentgenol 2007;189:913–21.
[10] Sha DD, Sutton JP. Towards automated enhancement, segmentation and classification of digital brain images using networks of networks. Inform Sci 2001;138:45–77.
[11] Vincent L, Soille P. Watersheds in digital spaces: an efficient algorithm based on immersion simulations. IEEE Trans Pattern Anal Mach Intell 1991;13:583–98.
[12] Parvati K, Prakasa Raso BS, Mariya Das M. Image segmentation using gray-scale morphology and marker-controlled watershed transformation. Discrete Dynamics in Nature and Society 2008;2018:1–8.
[13] Swets JA. Measuring the accuracy of diagnostic systems. Science 1988;240:1285–93.
[14] Unal I. Defining an optimal cut-point value in roc analysis: an alternative approach. Comput Math Methods Med 2017;2017:3762651.
[15] Carass A, Roy S, Jog A, et al. Longitudinal multiple sclerosis lesion segmentation: resource and challenge. NeuroImage 2017;148:77–102.
[16] Goldberg-Zimring D, Achiron A, Miron S, Faibel M, Azhari H. Automated detection and characterization of multiple sclerosis lesions in brain MR images. Magn Reson Imaging 1998;16:311–8.
[17] Khayati R, Vafadust M, Towhidkhah F, Nabavi SM. A novel method for automatic determination of different stages of multiple sclerosis lesions in brain MR FLAIR images. Comput Med Imaging Graph 2008;32:124–33.
[18] Shah M, Xiao Y, Subbanna N, Francis S, Arnold DL, Collins DL, et al. Evaluating intensity normalization on MRIs of human brain with multiple sclerosis. Med Image Anal 2011;15:267–82.
[19] Mussurakis S, Buckley DL, Horsman A. Dynamic MRI of invasive breast cancer: assessment of three region-of-interest analysis methods. J Comput Assist Tomogr 1997;21:431–8.
[20] Baltzer PA, Dietzel M, Vaq T, et al. Can color-coded parametric maps improve dynamic enhancement pattern analysis in MR mammography? RöFo-Fortschritte auf dem Gebiet der Röntgenstrahlen und der bildgebenden Verfahren 2010;18:254–60.
[21] Baltzer PA, Renz DM, Kullniq PE, Gajda M, Camara O, Kaiser WA. Application of computer-aided diagnosis (CAD) in MR mammography (MRM): do we really need whole lesion time curve distribution analysis? Acad Radiol 2009;16:435–42.
[22] William TC, De Martini WB, Partridge SC, Peacock S, Lehman CD. Breast MR imaging: computer-aided evaluation program for discriminating benign from malignant lesions. Radiology 2007;244:94–103.